Inorganic Chemistry

Article

pubs.acs.org/IC

Bifunctional Mesoporous Zirconium Phosphonates for Delivery of Nucleic Acids

Yan Tang,[†] Yubao Ren,[†] and Xin Shi*

Institute of Chemistry for Functionalized Materials, School of Chemistry and Chemical Engineering, Liaoning Normal University, 850 Huanghe Road, Dalian 116029, China

Supporting Information

ABSTRACT: The bifunctional mesoporous zirconium phosphonates (ZrBFs) were synthesized through surfactant-assisted co-condensation of $ZrCl_4$ with two different phosphonic acids, both 1-phosphomethylproline (H_3PMP) and 1,4-bis(phosphomethyl)-piperazine (BPMP), in a one-pot procedure. The L-proline group of H_3PMP and piperazine group of BPMP in the frameworks endow ZrBFs with pH-controllable release function and high cell penetration capability, which was derived from the reversible protonation−deprotonation of L-proline groups and piperazine groups on the mesoporous walls under different pH values (pH sensitivity) as well as further functionalization with biological modifiers via the carboxyls in L-proline groups on the outer surface (functionalizability), respectively. ZrBFs, possessing cationic frameworks once formed, exhibit high payload for salmon sperm DNA as model nucleic acid owing to strong electrostatic attraction between them. On the basis of pH-sensitive ZrBFs carriers and assisted by lag-time films coating, the time- and pH-controlled oral colon-targeted nucleic acid delivery systems have been developed, which can carry most of the loaded salmon sperm DNA to the colon under dual control, time control and pH value control. Furthermore, salmon sperm DNA can remain intact during delivery, as evidenced by the fact that the released salmon sperm DNA in the pH transition release experiment still retain its structural integrity and native conformation. Also, fluorescence spectra demonstrate that ZrBFs can be further functionalized with a cell-penetrating peptide of octaarginine (R8) via the carboxyls in L-proline groups of H_3PMP on the outer surface using a coupling agent, which will enhance the penetration capability of ZrBFs through biomembranes. ZrBFs have a potential application as a new kind of carrier in oral delivery of nucleic acids targeting the colon for gene therapy of colon-related diseases due to their unique bifunctionality.

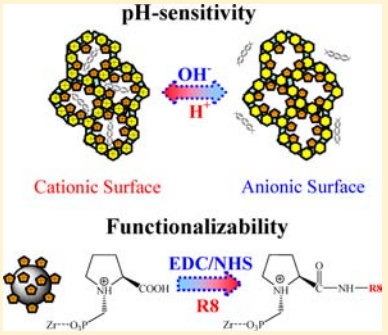

1. INTRODUCTION

With rapid progress in biotechnology and biomedicine, emerging therapeutic roles of nucleic acids have attracted a great deal of attention. However, delivery of nucleic acids to the body still remains a major challenge. Unlike other biopharmaceutics (such as amino acids, peptides and proteins, enzymes etc.), nucleic acids cannot be directly administered through injection and should be prepared through sophisticated pharmaceutical technology in order to protect nucleic acids against degradation of nuclease in the body after injection. Moreover, lack of targeting in the delivery of nucleic acids is also an obstacle. It is noteworthy that nucleic acids are not sensitive to digestive enzymes in the gastrointestinal tract (GIT), which might make oral delivery of nucleic acids feasible. To our knowledge, oral delivery of peptides and proteins has been a research focus in the field of an oral colon-targeted drug delivery system. Although many efforts have been made in developing an oral colon-targeted peptide and protein delivery system,[1−4] there are still a lot of challenges in delivery efficiency, bioactivity, and bioavailability. Inevitably, oral delivery of nucleic acids could encounter these challenges in the same way.

Mesoporous silicas are considered as a possible option of carriers for drug delivery due to their excellent chemical stability and physiochemical properties.[5−24] Commonly, mesoporous silicas as drug carriers release drug in a sustained-release method through adjustment of mesopore size and shape as well as modification of the mesopore wall with metal ions or organic groups.[9−16] Recently, mesoporous silicas were also used to develop pH-responsive drug delivery system targeting the intestine by incorporating trimethylammonium functional groups into mesopore walls wherein trimethylammonium groups adsorb anionic drugs through electrostatic attraction (trimethylammonium$^+$−drug$^-$), while deprotonated silanol groups increase drug release by electrostatic repulsion (Si−O$^-$−drug$^-$) at neutral pH.[17,18] Besides, combination of mesoporous silicas with coating technology has been developed for pH-controlled drug delivery systems targeting the intestine via coating pH-sensitive materials on drug-loaded mesoporous silicas.[19−24] It is worth mentioning that Kawi's group reported a pH-controllable drug delivery system for bovine serum albumin (BSA) by coating pH-sensitive poly(acrylic acid) (PAA) on BSA-loaded amine-functionalized SBA-15, in which BSA was released at the higher pH value of 7.4 rather than at the lower pH value of 1.2. They deemed that such a novel drug delivery

Received: September 27, 2012
Published: January 24, 2013

   dx.doi.org/10.1021/ic3020942 | Inorg. Chem. 2013, 52, 1388−1397

system could have potential application for targeted oral delivery of therapeutic proteins since the PAA coating can protect proteins from acidic conditions present in the stomach and trigger release of proteins at sites like the small intestine or colon.[24]

Oral delivery of nucleic acids requires that the delivery system should protect nucleic acids passing through GIT and carry nucleic acids targeting organ/tissue. The oral colon-targeted nucleic acid delivery system may be an optimal candidate because it not only can protect nucleic acids against damage resulted from acidic medium in the stomach but also can control nucleic acids to target colonic focus, which might make for gene therapy of colon-related diseases. In this paper, bifunctional mesoporous zirconium phosphonates (ZrBFs) were designed and used as carriers, assisted by lag-time films coating, to develop a time- and pH-controlled oral colon-targeted nucleic acid delivery system. Mesoporous phosphonates possess unique tailorable frameworks through adjusting either/both metal or/and phosphonic acid to roll up multiple applications into one, such as both catalyst and ion exchanger,[25,29a] both catalyst and adsorber.[29b] To the best of our knowledge, synthesis of mesoporous phosphonates for delivery of nucleic acids has not been found so far.[25−29,36,37] Here, two phosphonic acids of 1-phosphomethylproline (H_3PMP) and 1,4-bis(phosphomethyl)piperazine (BPMP) were simultaneously incorporated into the frameworks of mesoporous zirconium phosphonates wherein L-proline groups of H_3PMP and piperazine groups of BPMP endow the materials with bifunctionality, i.e., pH sensitivity and functionalizability. ZrBFs as carriers, the mesopore will accommodate nucleic acids and the pH sensitivity will control release of nucleic acids as well as the functionalizability will enhance carriers' cell penetration capability. In addition, the lag-time films coating can protect nucleic acids from gastric acid in the stomach and also be adjusted to control the lag time to avoid loss of nucleic acids in advance. Using salmon sperm DNA as model nucleic acid below, the adsorption isotherms and kinetics of ZrBFs were investigated in detail as well as in vitro release profiles of salmon sperm DNA-loaded ZrBFs coated with different lag-time films were studied to value an oral colon-targeted nucleic acid delivery system based on ZrBFs.

2. EXPERIMENTAL SECTION

Materials and Methods. 1-Phosphomethylproline (H_3PMP)[30] and 1,4-bis(phosphomethyl)piperazine (BPMP)[31] were prepared by modifications of the reported methods. Tetrachloride zirconium ($ZrCl_4$, 99.5%) was purchased from Alfa Aesar; sodium dodecyl sulfate (SDS), tetrahydrofuran (THF), sodium hydroxide, triethylamine, anhydrous ethanol, hydrochloric acid (36−38%), sodium phosphate, sodium dihydrogen phosphate, disodium hydrogen phosphate, ethylcellulose (EC), diethyl phthalate, PEG 400, glucose, glycine, Tween 20, and dimethylformamide (DMF) were analytical grade and purchased from Tianjin Chemical reagents. *N*-(3-Dimethylaminopropyl)-*N*′-ethylcarbodiimide hydrochloride (EDC) and *N*-hydroxysuccinimide (NHS) were bought from Sigma-Aldrich. All of the above materials were directly used without further purification. Salmon sperm DNA for adsorption and release was obtained from Wako Pure Chemical Industries Ltd. and used as received (absorbances of 260 and 280 nm were measured, and A_{260nm}/A_{280nm} was about 1.8, indicating the high purity of salmon sperm DNA without contamination of protein). Salmon sperm DNA for the CD spectrum and 9,10-phenanthraquinone (>99%) were purchased from Sigma-Aldrich and used without purification. Octaarginine (R8) was ordered and prepared by Apeptide Co. Ltd. and used as received.

N_2 adsorption−desorption isotherms were obtained at 77 K on a Micromeritics ASAP 2010 automated analyzer. Surface areas were estimated according to the BET method, and pore size distributions were calculated based on the Barrett−Joyner−Halenda (BJH) method. Scanning electron microscopy (SEM) was performed on a Quanta 200F electron microscope (30 kV). Transmission electron microscopy (TEM) was done using a JEM-2010 at an acceleration voltage of 100 KV. ^{31}P (161.8 MHz) MAS NMR spectrum and ^{13}C (100.5 MHz) CP/MAS NMR spectra were measured on a Bruker DRX-400 spectrometer. The chemical shift of ^{31}P NMR was referenced to $NH_4H_2PO_4$. CD spectra were conducted on a Jasco J-810 circular dichroism spectropolarimeter. Fluorescence spectra were obtained on Hitachi F-7000 fluorescence spectrometer.

Synthesis. Bifunctional mesoporous zirconium phosphonates were synthesized through a surfactant-assisted procedure using two phosphonic acids with different functional groups, 1-phosphomethylproline (H_3PMP) and 1,4-bis(phosphomethyl)piperazine (BPMP), as well as zirconiuim precursor of tetrachloride zirconium ($ZrCl_4$) in the presence of sodium dodecyl sulfate (SDS) under weakly acidic conditions. In a typical synthesis, H_3PMP (1.25 mmol, 0.261 g) and BPMP (0.625 mmol, 0.171 g) were added to 20 mL of distilled water containing a desired amount of SDS under constant stirring and remained stirring for a period of time. A mixture of $ZrCl_4$ (5 mmol, 1.165 g) in 5 mL of tetrahydrofuran (THF) was dropwise added to the above aqueous solution under vigorous stirring. Then the pH of the mixture was adjusted to ca. 4.0 with NaOH solution followed by triethylamine. After stirring for 1 h, the mixture was transferred to a Teflon-lined stainless steel autoclave and heated at 160 °C for 24 h. The white powder was filtered off, washed with distilled water, and dried at 60 °C in a vacuum oven. Surfactant was extracted by stirring 1 g of the powder in 80 mL of anhydrous ethanol containing HCl solution (2 mol/L, 1 mL) at room temperature for 8 h. The molar ratio of the initial reactants was SDS:$ZrCl_4$:H_3PMP:BPMP = *n*:4:1:0.5 (*n* = 1, 2, 4, and 8). Hereafter, these mesoporous zirconium phosphonates comprised of two kinds of functional phosphonates, namely, bifunctional mesoporous zirconium phosphonates, were designated as ZrBF-*n*, where *n* (*n* = 1, 2, 4, and 8) is the molar ratio of SDS/H_3PMP in the initial reactants.

Adsorption of Salmon Sperm DNA. All solid materials were dried at 80 °C for 24 h in a vacuum oven before adsorption of salmon sperm DNA. Adsorption isotherm were obtained by preparing a series of salmon sperm DNA solutions with concentration ranging from 6 to 400 μg/mL in pure water. In each adsorption experiment, 10 mg of ZrBF-*n* sample was added to 10 mL of salmon sperm DNA solutions with different concentration, and the resulting mixture was continuously shaken in a shaking bath at room temperature for 24 h. Supernatant was separated from the solid materials by repetitious centrifugation, and salmon sperm DNA content in the supernatant was measured using UV absorption at 260 nm.

The kinetics of salmon sperm DNA adsorption were investigated by suspending 10 mg of sample in salmon sperm DNA solution (150 μg/mL, 10 mL). The mixture was shaken in a shaking bath at room temperature for different intervals and measured periodically. For each measurement, the upper solution was separated from the solid materials by repetitious centrifugation, and salmon sperm DNA content of upper limpid solution was measured using UV absorption at 260 nm.

The amount of salmon sperm DNA adsorbed into ZrBF-*n* was calculated by the difference of the concentration of salmon sperm DNA before and after adsorption according to the following equation: $M = [C_iV - C_eV]/m$, where M (μg/mg) is the amount of adsorbed salmon sperm DNA per microgram of materials, C_i (μg/mL) is the initial concentration of salmon sperm DNA, C_e (μg/mL) is the concentration of salmon sperm DNA in the upper limpid solution after adsorption, V (mL) is the volume of salmon sperm DNA solution, and m (mg) is the weight of materials.

Adsorption Isotherm Models. Two isotherm models, the Langmuir model[32] and Freundlich model,[33] were applied in our research to establish the most appropriate adsorption isotherm. The Langmuir model is an ideal monolayer sorption on homogeneous

dx.doi.org/10.1021/ic3020942 | Inorg. Chem. 2013, 52, 1388−1397

surface and has several assumptions as follows: adsorption takes place at specific homogeneous sites within the adsorbent; all adsorption sites are identical and energetically equivalent; each site can accommodate only one molecule or atom; there is no interaction between adsorbates. The saturated capacity can be represented by the following expression, where q_e is the solid-phase sorbate concentration at equilibrium (μg/mg), C_e is the sorbate concentration in the aqueous phase at equilibrium (μg/mL), and K_L (mL/mg) and α_L (mL/μg) are Langmuir parameters.

$$q_e = \frac{K_L \times C_e}{1 + \alpha_L \times C_e} \quad (1)$$

A linear expression of the Langmuir equation can be represented by

$$\frac{C_e}{q_e} = \frac{1}{K_L} + \frac{\alpha_L}{K_L} \times C_e \quad (2)$$

with the expression K_L/α_L giving the theoretical monolayer saturation capacity (Q_0, μg/mg).

The Freundlich model can be applied to nonideal sorption on heterogeneous surfaces as well as multilayer sorption and is expressed by the following equation

$$q_e = K_F \times C_e^{1/n} \quad (3)$$

where q_e is the solid-phase sorbate concentration at equilibrium (μg/mg), C_e is the sorbate concentration in the liquid phase at equilibrium (μg/mL), K_F is the Freundlich parameter [mL/($\mu g^{1-1/n}$·mg)], and $1/n$ (b_F) is the heterogeneity factor. A linear form of the Freundlich expression can be obtained by taking logarithms of eq 4.

$$\ln q_e = \ln K_F + \frac{1}{n} \times \ln C_e \quad (4)$$

Adsorption Kinetic Models. The most common kinetics models, pseudo-first-order and pseudo-second-order reaction rate equation, were adopted in order to investigate the adsorption mechanism based on experimental data. The pseudo-first-order kinetic equation is given as follows

$$\ln(q_e - q_t) = \ln q_e - k_1 t \quad (5)$$

where q_t is the amount of adsorbate adsorbed at any time (μg/mg), q_e is the adsorptive capacity at equilibrium (μg/mg), k_1 is the rate constant (1/min), and t is the time (min). The plot of $\ln(q_e - q_t)$ against t should give a straight line with slope $-k_1$ and intercept $\ln q_e$.

The pseudo-second-order kinetic equation is expressed as

$$\frac{t}{q_t} = \frac{1}{k_2 q_e^2} + \frac{t}{q_e} \quad (6)$$

where q_t is the amount of adsorbate adsorbed at any time (μg/mg), q_e is the adsorptive capacity at equilibrium (μg/mg), k_2 is the rate constant (mg/μg·min), and t is the time (min). The k_2 and adsorptive capacity at equilibrium (q_e) can be obtained experimentally from the slope and intercept of the plot of t/q_t versus t.

Lag-Time Films Coating. Some amount of salmon sperm DNA-loaded ZrBF-2 was pressed into a core tablet under 3.0 MPa uniaxial pressure and weighed. The core tablet was then inserted into 0.6 g of glucose (glycine for CD spectroscopy) and pressed again into a 13 mm × 2.8 mm tablet under 3.0 MPa uniaxial pressure. The coating solution was prepared by dissolving 3.0 g of ethylcellulose (EC) in 100 mL of anhydrous ethanol containing 0.6 g of diethyl phthalate (20% of EC, W/W) and 0.45 g of PEG 400 (15% of EC, W/W) under stirring at room temperature. The salmon sperm DNA-loaded ZrBF-2 tablets were dip coated with the above coating solution. Tablets were repeatedly coated with coating solution two times, three times, four times, or five times. After each dip coating, the coated tablets were dried at room temperature for 20 min.

Release of Salmon Sperm DNA. The release behaviors of salmon sperm DNA from salmon sperm DNA-loaded ZrBF-2 coated with different lag-time films during the transition from pH 1.2 to pH 7.4 were carried out in the simulated gastric fluid (diluted HCl solution, pH 1.2) for 3 h, then 0.2 mol/L sodium phosphate solution to the above acidic solution was added, and the pH value was adjusted to 7.4 ± 0.05 with 2 mol/L sodium hydroxide solution. Samples of the release medium were taken for analysis at predetermined time points, and salmon sperm DNA contents were measured using UV absorption at 260 nm.

Functionalization of ZrBFs. EDC (0.0767 g) and NHS (0.0116 g) were separately dissolved in 1 mL of pure water and mixed together, forming a uniform clear solution. A 10 mg amount of salmon sperm DNA-loaded ZrBF-2 was added to EDC/NHS solution, and the mixture was shaken by hand several minutes. After centrifugation, the solid was repeatedly washing with phosphate buffer (0.1 mol/L of NaH_2PO_4–Na_2HPO_4, pH = 7.0). A solution of octaarginine (R8: 0.3 mg/mL, 1.0 mL) was added to the above active salmon sperm DNA-loaded ZrBF-2, and the mixture was shaken in a shaking bath at room temperature for 24 h. Solid was separated from solution by centrifugation and washed with 2‰ of Tween 20. Then the solid was repeatedly washed with phosphate buffer (0.1 mol/L of NaH_2PO_4–Na_2HPO_4, pH = 7.0) until the wash solution was clear. The functionalized product, named salmon sperm DNA-loaded ZrBF-2-R8, was dried at room temperature.

Fluorimetric Procedure. *Preparation of Calibration Graph.* A series of R8 solutions was prepared with concentration in the range from 200 to 500 μg/mL. A 20 μL amount of R8 solution was placed in a 25 mL calibrated flask, and 2.5 mL of 9,10-phenanthraquinone reagent (2 μg/mL in dimethylformamide) was added followed by NaOH solution (1 mol/L, 0.25 mL). The mixture was allowed to stand for 45 min at room temperature; then HCl solution (1 mol/L, 0.25 mL) was addded to the above mixture and made up to volume with pure water.[34] The fluorescence intensity was measured at once with an excitation wavelength of 260 nm and emission wavelength of 405 nm. A linear relationship between fluorescence intensity and concentration of R8 was found: $F = 6.944C$ (μg/mL) + 283, R^2 = 0.99511, linearity range 200–400 μg/mL.

Determination of R8 in Salmon Sperm DNA-Loaded ZrBF-2-R8. A 1 mg amount of salmon sperm DNA-loaded ZrBF-2-R8 was dissolved in 50 μL of 1 mol/L NaOH solution. A 20 μL amount of the above solution was placed in a 25 mL calibrated flask; then the following procedure was the same as that of preparing the calibration graph. The contrast test was also conducted by dissolving 1 mg of salmon sperm DNA-loaded ZrBF-2 in 50 μL of 1 mol/L NaOH solution, and the subsequent fluorimetric procedure was the same as above.

3. RESULTS AND DISCUSSION

3.1. Synthesis and Characterization. ZrBFs were synthesized through one-pot co-condensation of two phosphonic acids with different functional groups, 1-phosphomethylproline (H_3PMP) and 1,4-bis(phosphomethyl)piperazine (BPMP) (Scheme 1), with $ZrCl_4$ in the presence of anionic surfactant SDS under weakly acidic conditions. The diphosphonic acid of BPMP embeds in mesopore walls since its two phosphonate groups incline to coordinate to zirconium at the same time, whereas the phosphonic acid of H_3PMP stretches out to the mesopores for coordination of one phosphonate

Scheme 1. Molecular Structures of 1-Phosphomethylproline (H_3PMP) and 1,4-Bis(phosphomethyl)piperazine (BPMP)

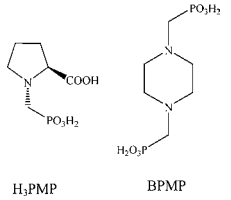

H_3PMP BPMP

dx.doi.org/10.1021/ic3020942 | Inorg. Chem. 2013, 52, 1388–1397

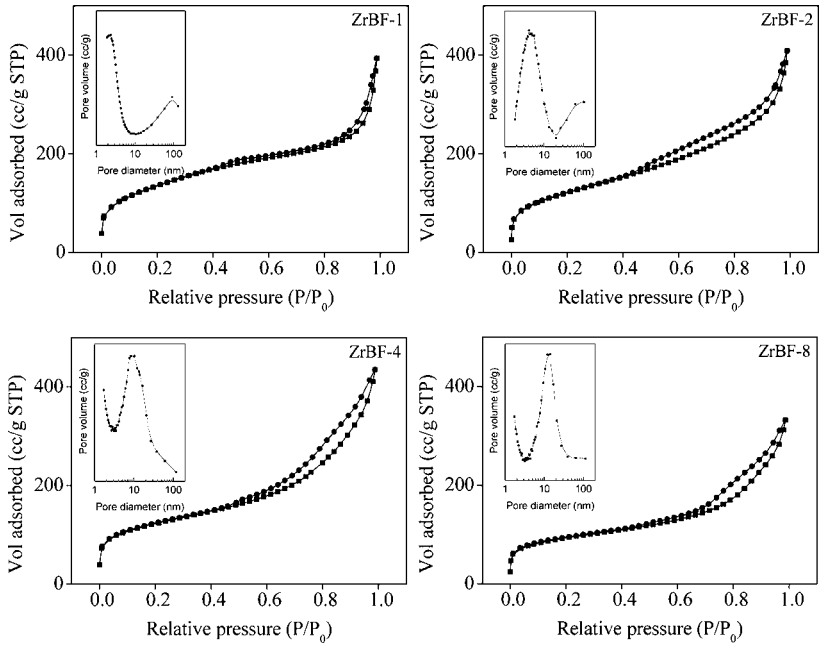

Figure 1. Nitrogen sorption isotherms of surfactant-extracted ZrBF-*n* (*n* = 1, 2, 4, and 8; (inset) shows the pore size distribution curve based on adsorption branch).

group to zirconium, which favors improving the textural properties of ZrBFs. The N_2 adsorption−desorption isotherms of ZrBF-*n* samples are shown in Figure 1. ZrBF-1 sample displays an isotherm pattern on the border between type I and type IV with a sharp N_2 uptake at relative pressure close to the saturation vapor pressure which suggests the existence of larger mesopores and possible macropores. ZrBF-*n* (*n* = 2, 4, and 8) samples synthesized with higher SDS amount exhibit a type IV isotherm pattern with H3 hysteresis loop, which indicates the materials have mesoporous structure. The H3 hysteresis loops without leveling off at a relative pressure (P/P_0) near 1.0 suggests the presence of interparticle void spaces,[35] as evidenced by loose assemblage of small particles among samples in SEM images (Figure S1, Supporting Information). SEM images of ZrBF-*n* samples show all materials are blocks aggregated from irregularly shaped spheres (Figure S1, Supporting Information). From ZrBF-2 to ZrBF-8, the hysteresis loop shifts to higher relative pressure (P/P_0), implying pore diameter expansion at high SDS amount. The largest pore diameter of 14.0 nm can be obtained when the amount of SDS increases to a molar ratio SDS/H_3PMP of 8. The pore volume also increases with the increase of SDS amount and reaches the maximum at SDS/H_3PMP ratio of 4. However, increasing the amount of SDS will cause the decrease of the surface area (Table 1). The nitrogen adsorption amount rapidly increases at a relative pressure of P/P_0 less than 0.1 for all ZrBF-*n* samples, indicating that the materials have micropores besides mesopores. The results of N_2 isotherms show that the textural structure of the materials is affected by SDS amount in the initial reactants to a great extent. Moreover, ZrBF-*n* samples except for ZrBF-8 exhibit high surface area (>400 m^2/g) and large pore volume (>0.60 cm^3/g), which may be due to the cooperation of two phosphonic acids in the synthesis, improving the textural properties of ZrBFs.

The ZrBF-*n* samples exhibit no diffraction peak in the low-angle region from the powder XRD pattern, showing ZrBFs are disordered mesoporous materials. The TEM image (Figure S2, Supporting Information) displays irregularly arranged worm-like pores throughout the material, which is consistent with the result of powder XRD, further confirming that the samples have a disordered mesoporous structure.

As shown in Figure 2, the ^{31}P MAS NMR spectrum of ZrBF-2 presents a resonance signal centered at about 0 ppm, which could be assigned to the organic phosphorus species in the framework. The chemical shift of the organic phosphorus species in the mesoporous solids constructed from H_3PMP and BPMP was centered at 0 and 1.0 ppm, respectively.[36,37] Thus, a slightly broadened resonance signal centered at about 0 ppm in Figure 2 should result from the overlap of two resonance

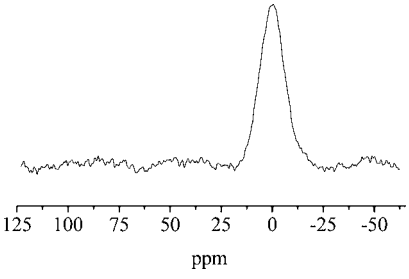

Figure 2. ^{31}P MAS NMR spectrum of surfactant-extracted ZrBF-2.

Table 1. Physicochemical Data of Surfactant-Extracted ZrBF-*n* (*n* = 1, 2, 4, and 8)

	SDS:$ZrCl_4$:H_3PMP:BPMP	BET surface area (m^2/g)	pore volume (cm^3/g)	pore size BJH (nm)
ZrBF-1	1:4:1:0.5	490	0.61	2.4
ZrBF-2	2:4:1:0.5	437	0.63	4.7
ZrBF-4	4:4:1:0.5	432	0.67	10.4
ZrBF-8	8:4:1:0.5	325	0.51	14.0

dx.doi.org/10.1021/ic3020942 | Inorg. Chem. 2013, 52, 1388−1397

signals, which can separately be attributed to the organic phosphorus species of H_3PMP and BPMP.

The ^{13}C CP/MAS NMR spetrum of ZrBF-2 displays a series of resonance signals at 22.8, 28.7, 50.2, 53.6, 56.5, 72.1, and 172.2 ppm (Figure 3). Two signals at 50.2 and 53.6 ppm are

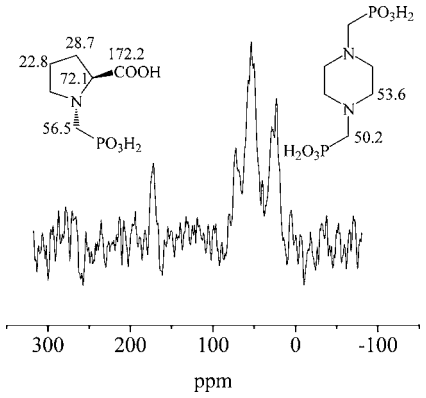

Figure 3. ^{13}C CP/MAS NMR spectrum of surfactant-extracted ZrBF-2.

similar to that in the ^{13}C CP/MAS NMR spectrum of BPMP (Figure S3, Supporting Information). The signal at 50.2 ppm can be assigned to the C atoms of CH_2 groups linked with phosphonate in BPMP since the phosphonate group causes the resonance signal of the neighboring C atom to shift downfield. Then the resonance at 53.6 ppm is attributable to the C atoms of CH_2 groups of the piperazine ring in BPMP. In addition, the signal at 172.2 ppm is associated with the C atom of carboxyl in H_3PMP. The resonance at 72.1 ppm can be assigned to the C atom of the CH group connected with carboxyl in H_3PMP, while the signal at 56.5 ppm is attributed to the C atom of the CH_2 group linked with phosphonate in H_3PMP. The other two signals at 22.8 and 28.7 ppm can be attributable to C atoms of CH_2 groups of the pyrrolidine ring in H_3PMP. The resonance signal related with the last CH_2 group of the pyrrolidine ring in H_3PMP should be located at about 59 ppm,[38] however, and cannot be observed in Figure 3. The signal at about 59 ppm should be overlaid by another signal at 56.5 ppm because two similar signals (59 and 56 ppm) overlapped in ref 38. The results of ^{13}C CP/MAS NMR show that two phosphonic acids, H_3PMP and BPMP, can retain their integrated structure during synthesis and solvent abstraction of surfactant. Furthermore, the resonance signals correlated to C atoms of SDS do not appear in the ^{13}C CP/MAS NMR spectrum, which indicates that surfactant of SDS can be almost completely abstracted in the surfactant removal process.

^{31}P MAS NMR and ^{13}C CP/MAS NMR confirm that the phosphonic acid of H_3PMP and diphosphonic acid of BPMP have been simultaneously incorporated into the frameworks of ZrBFs. The L-proline groups and piperazine groups in the frameworks cause ZrBFs to possess bifunctionality, i.e., pH sensitivity and functionalizability. As illustrated in Scheme 2, the reversible protonation−deprotonation of L-proline groups of H_3PMP in the mesopores and piperazine groups of BPMP on the pore walls under different pH values brings ZrBFs with pH-sensitive cationic−anionic surface properties (pH sensitivity), which endows ZrBFs with pH-controllable release function. Meanwhile, further functionalization of the carboxyls in L-proline groups of H_3PMP on the outer surface with special biomolecules occurs, such as a cell-penetrating peptide of octaarginine (R8) (functionalizability), which will help to enchance the penetration capability of ZrBFs through biomembranes. Additionally, L-proline as natural amino acid makes ZrBFs with good biocompatibility.

3.2. Adsorption of Salmon Sperm DNA. ZrBFs exhibit cationic frameworks once formed because L-proline groups of

Scheme 2. Illustration of ZrBFs' Bifunctionality, pH Sensitivity, and Functionalizability

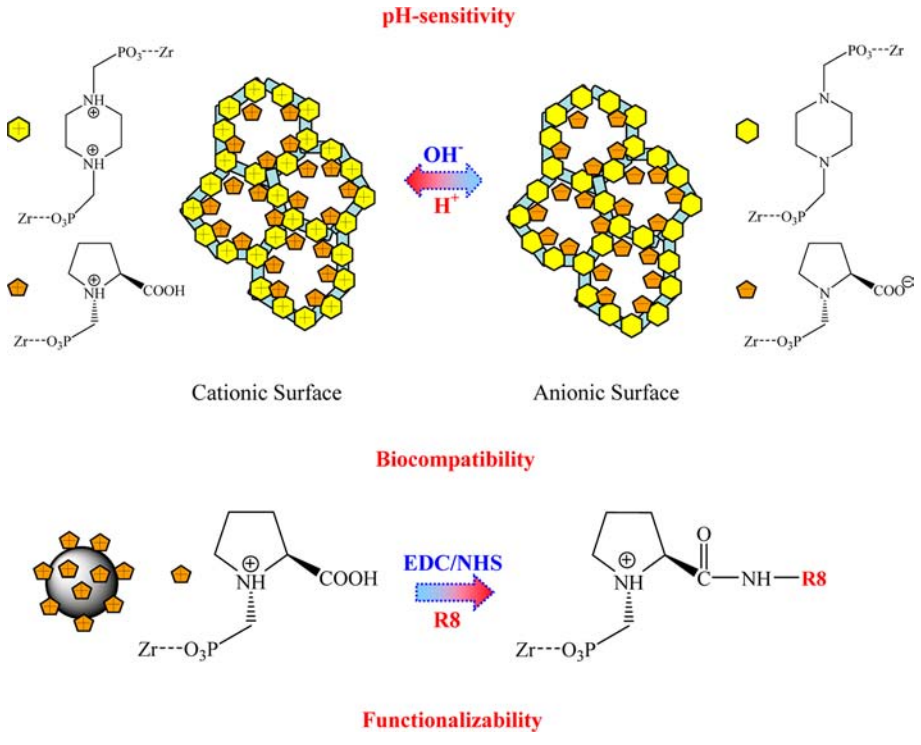

dx.doi.org/10.1021/ic3020942 | Inorg. Chem. 2013, 52, 1388−1397

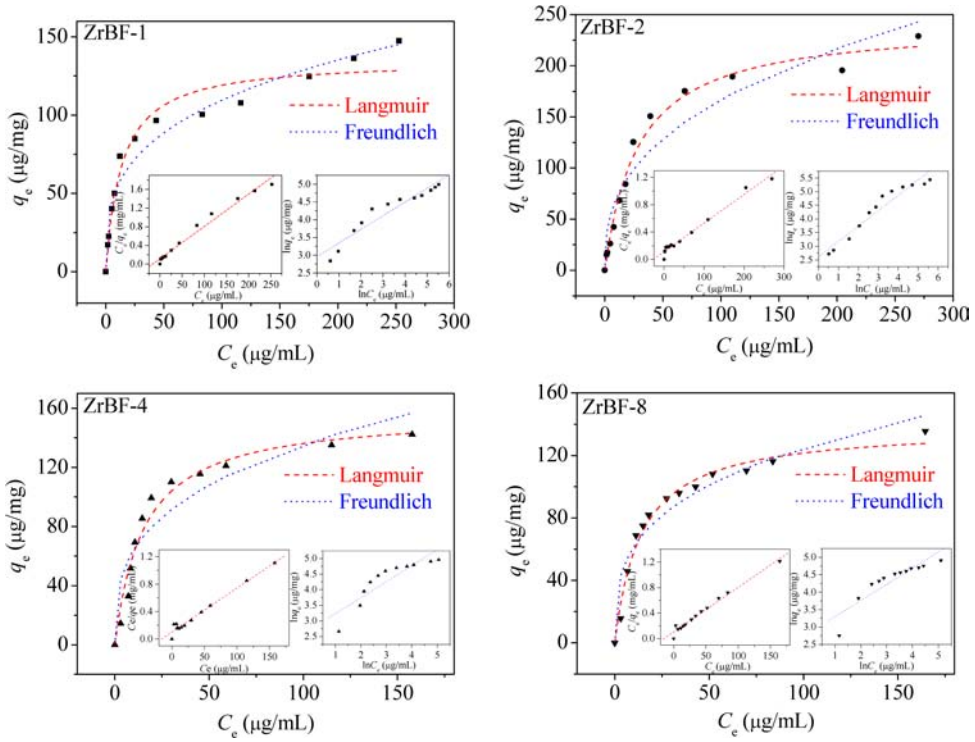

Figure 4. Adsorption of salmon sperm DNA into ZrBF-*n* (*n* = 1, 2, 4, and 8) (time = 24 h, temperature = 25 °C). Scatter dots show experimental equilibrium adsorption data of ZrBF-*n* materials for salmon sperm DNA. Dashed curves represent a fit of the experimental data by employing the Langmuir model. Dotted curves express a fit of the experimental data using the Freundlich model.

H_3PMP and piperazine groups of BPMP were protonated by a mass of hydrochloric acid resulting from hydrolysis of $ZrCl_4$ in the synthesis. Thus, ZrBFs were directly used in the adsorption of salmon sperm DNA without further treatment. The equilibrium adsorption data of ZrBF-*n* for salmon sperm DNA are displayed in Figure 4. To establish the most appropriate adsorption isotherm, the correlation of the equilibrium adsorption data was carried out using two theoretical adsorption models, the Langmuir model and Freundlich model. The equilibrium adsorption data of ZrBF-*n* for salmon sperm DNA were analyzed according to the linear form of the Langmuir equation (eq 2 in the Experimental Section) and Freundlich equation (eq 4 in the Experimental Section), respectively, and the linear fit plots of ZrBF-*n* for salmon sperm DNA are shown in the left and right insets of Figure 4. From the left insets in Figure 4, it can be obviously observed that all isotherms of ZrBF-*n* are linear over the whole concentration range. The correlation coefficients of ZrBF-*n* for salmon sperm DNA are also extremely high (Table 2). In other words, the adsorption behaviors of ZrBF-*n* for salmon sperm DNA can be accurately described by the Langmuir isotherm, which indicates that adsorption of salmon sperm DNA into ZrBF-*n* is a single-layered sorption with little intermolecular interaction between salmon sperm DNA, whereas there is rather large deviation from linearity for ZrBF-*n* in the whole concentration range from the right insets in Figure 4 and the poor correlation coefficients of ZrBF-*n* for salmon sperm DNA as listed in Table 3, showing that the experimental data of ZrBF-*n* for salmon sperm DNA do not fit the Freundlich model and multilayer sorption with significant intermolecular interaction between salmon sperm DNA does not exist in the adsorption of salmon sperm DNA into ZrBF-*n*. Figure 4 also shows the comparison of isotherms, separately fitted using the Langmuir model (dashed curves) and Freundlich model (dotted curves), with experimental equilibrium adsorption data (scatter dots) of ZrBF-*n* for salmon sperm DNA.

Table 2. Langmuir Sorption Isotherm Parameters of ZrBF-*n* (*n* = 1, 2, 4, and 8) for Salmon Sperm DNA

	K_L (mL/mg)	a_L (mL/μg)	R^2	Q_0 (μg/mg)	Q_S (μg/m^2)
ZrBF-1	8.55578	0.05912	0.99022	144.7	0.30
ZrBF-2	8.95576	0.03753	0.99098	238.6	0.55
ZrBF-4	9.99201	0.06435	0.98825	155.2	0.36
ZrBF-8	9.47867	0.06616	0.99059	143.3	0.44

Table 3. Freundlich Sorption Isotherm Parameters of ZrBF-*n* (*n* = 1, 2, 4, and 8) for Salmon Sperm DNA

	b_F	K_F [mL/(μg$^{1-1/n}$·mg)]	R^2
ZrBF-1	0.38398	19.31631	0.95456
ZrBF-2	0.56226	13.67692	0.9654
ZrBF-4	0.51077	15.23568	0.88503
ZrBF-8	0.46305	17.03807	0.89718

ZrBF-2 exhibits the largest equilibrium monolayer capacity (Q_0) of 238.6 μg/mg for salmon sperm DNA among all ZrBF-*n* samples (Table 2). Although ZrBF-1 has the highest surface area and ZrBF-4 possesses the largest pore volume among ZrBF-*n*, their equilibrium monolayer capacities are less than that of ZrBF-2. ZrBF-8, despite possessing the largest pore diameter among ZrBF-*n*, adsorbs less salmon sperm DNA than ZrBF-2. ZrBF-1 clearly adsorbs less salmon sperm DNA than the other materials, probably due to the pore diameter limitation hindering diffusion of salmon sperm DNA into the

dx.doi.org/10.1021/ic3020942 | Inorg. Chem. 2013, 52, 1388−1397

pore. The largest pore volume (ZrBF-4) and pore diameter (ZrBF-8) do not favor the adsorption capacity because of a single-layered sorption of salmon sperm DNA into ZrBF-*n*. To further understand the adsorption behaviors of ZrBF-*n* for salmon sperm DNA, the equilibrium monolayer capacities of the samples are compared relative to their surface areas. The specific adsorption capacity ($Q_S = Q_0/S_B$) of ZrBF-*n* except for ZrBF-2 increases with the surface area decreasing (Table 2), indicating that the loading capacity of the materials is not determined by the surface area. ZrBF-2 adsorbs much more salmon sperm DNA than ZrBF-3 though they have similar surface area and pore volume, which suggests that the adsorption capacity of the materials lies on a special pore diameter of about 5 nm. In general, DNA adopts a cylindrical structure with an estimated cross-sectional diameter of about 2 nm at room temperature. The pore size of 2.4 nm for ZrBF-1 is almost the equivalent of the molecular size of salmon sperm DNA, suggesting that the pore diameter limits diffusion of salmon sperm DNA into the pore to some extent, which results in ZrBF-1 adsorbing less salmon sperm DNA than the other materials. For ZrBF-4 and ZrBF-8, their pore size more than 10 nm is much larger than the molecular size of salmon sperm DNA and large enough to accommodate salmon sperm DNA; however, the larger pore size does not favor the adsorption amount of salmon sperm DNA on the condition that a single-layered sorption occurs. Moreover, the strong electrostatic repulsion between negatively charged salmon sperm DNA and its adjacent one causes salmon sperm DNA molecules to disperse as far as possible in the pore. ZrBF-2 with a pore diameter of 4.7 nm is large enough to hold salmon sperm DNA without serious diffusion resistance and pore confinement make salmon sperm DNA adsorbed into the pore maintain the packed arrangement. In other words, a pore diameter of about 5 nm just matches the molecular size of salmon sperm DNA, which improves the adsorption amount of salmon sperm DNA into ZrBF-2.

The adsorption kinetics of ZrBF-*n* for salmon sperm DNA are also studied as shown in Figure 5. From the profiles of adsorption kinetics, all samples of ZrBF-*n* can reach the equilibrium within 8 h. The comparatively slow adsorption of salmon sperm DNA into ZrBF-*n* may be due to the large dimension of salmon sperm DNA. The adsorption mechanism was investigated based on the kinetic experimental data by applying the two prevalently adopted kinetics models, pseudo-first-order and pseudo-second-order reaction rate equation. The adsorption rate data of ZrBF-*n* for salmon sperm DNA were analyzed according to the pseudo-first-order reaction rate equation (eq 5 in the Experimental Section) and pseudo-second-order reaction rate equation (eq 6 in the Experimental Section), respectively, and the linear fit plots of ZrBF-*n* for salmon sperm DNA are displayed in the left and right inset of Figure 5. The bad fitting as shown in the left inset of Figure 5 and the poor correlation coefficients as listed in Table 4 indicate that kinetic experimental data of ZrBF-*n* for salmon sperm DNA do not fit the pseudo-first-order kinetic model. However, the linear fitting is best (right inset in Figure 5), and the correlation coefficients are extremely high (Table 4), showing that the pseudo-second-order kinetics can finely describe the adsorption of salmon sperm DNA into ZrBF-*n*. The results of fit indicate that the sorption rests with adsorbents and adsorbate, more specifically, ZrBF-*n* exhibiting cationic surface properties at acidic or neutral conditions and salmon sperm DNA behaving negatively charged polyelectrolyte at physiological conditions. The strong electrostatic attraction between ZrBF-*n* and salmon sperm DNA forms a physisorption process which may be the rate-limiting step in the adsorption of salmon sperm DNA into ZrBF-*n*.

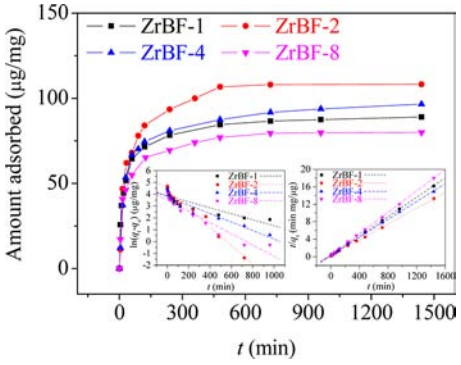

Figure 5. Adsorption kinetics of ZrBF-*n* (*n* = 1, 2, 4, and 8) for salmon sperm DNA (150 μg of salmon sperm DNA/1 mg of materials; temperature = 25 °C). (Insets) Linear fit according to the pseudo-first-order rate equation (left) and pseudo-second-order rate equation (right), respectively.

Table 4. Adsorption Kinetic Constants of ZrBF-*n* (*n* = 1, 2, 4, and 8) for Salmon Sperm DNA

	pseudo-first-order model		pseudo-second-order model	
	k_1 (1/min)	R^2	k_2 (mg/μg·min)	R^2
ZrBF-1	2.53×10^{-3}	0.90544	4.7×10^{-4}	0.99988
ZrBF-2	7.81×10^{-3}	0.98802	2.61×10^{-4}	0.99975
ZrBF-4	3.62×10^{-3}	0.95505	2.83×10^{-4}	0.9997
ZrBF-8	4.74×10^{-3}	0.96134	4.63×10^{-4}	0.99985

3.3. Release of Salmon Sperm DNA. The release behaviors of salmon sperm DNA-loaded ZrBF-2 without and with lag-time film coating were investigated in detail due to high payload of ZrBF-2 for salmon sperm DNA. Figure 6 shows salmon sperm DNA release profiles of uncoated salmon sperm DNA-loaded ZrBF-2 in the simulated gastric fluid (pH 1.2) and in the simulated intestinal fluid (pH 7.4). It is clear that the release of salmon sperm DNA from uncoated salmon sperm DNA-loaded ZrBF-2 in the simulated gastric fluid (pH 1.2) is extremely slow as compared with that in the simulated intestinal fluid (pH 7.4). In the simulated gastric fluid (pH

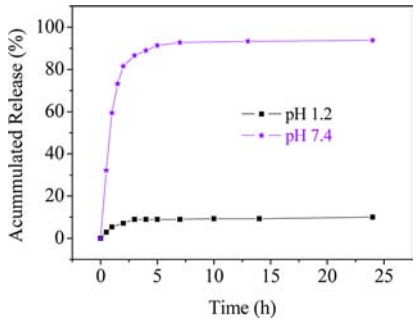

Figure 6. Release profiles of salmon sperm DNA-loaded ZrBF-2 in the simulated gastric fluid (pH 1.2) and in the simulated intestinal fluid (pH 7.4).

dx.doi.org/10.1021/ic3020942 | Inorg. Chem. 2013, 52, 1388−1397

1.2), only 8.9% of salmon sperm DNA is released within 3 h and the following release always hold the line on the release amount within 24 h. The small quantity of salmon sperm DNA release at pH 1.2 may be contributed from salmon sperm DNA that were adsorbed on the external surface instead of into the mesopore of ZrBF-2, whereas in the simulated intestinal fluid (pH 7.4) there is a burst release of salmon sperm DNA within 4 h, during which salmon sperm DNA could be released up to 89% of the loaded amount. The pH-controlled release result obtained above is believed to be due to pH sensitivity of ZrBF-2. Under acidic medium of pH 1.2, ZrBF-2 exhibiting cationic surface properties can firmly adsorb and hold negatively charged salmon sperm DNA in the mesopore through strong electrostatic attraction between them. Under weakly basic condition of pH 7.4, deprotonation of pyrrolidine rings and piperazine rings of H_3PMP and BPMP, respectively, on the mesopore walls results in ZrBF-2 losing surface positive charges accompanying the disappearing of the electrostatic attraction between ZrBF-2 and salmon sperm DNA. At the same time, the carboxyls in L-proline groups of H_3PMP on the mesopore walls deprotonate to form carboxylates with negative charges, which causes ZrBF-2 to display anionic surface properties. Consequently, the electrostatic repulsion between ZrBF-2 with anionic surface properties and negatively charged salmon sperm DNA accelerates the release of salmon sperm DNA from ZrBF-2.

The gastric emptying time has been reported to vary from 15 min to more than 3 h.[39] The small intestinal transit is surprisingly constant at 3−4 h,[40] and the maximum mean colonic transit time can reach 33 h for men and 47 h for woman.[41] Thus, in vitro release experiments were carried out in the simulated gastric fluid (pH 1.2) for 3 h (stomach 3 h) followed by in the simulated intestinal fluid (pH 7.4) for 51 h (small intestine 4 h and colon 47 h) to investigate release of salmon sperm DNA from salmon sperm DNA-loaded ZrBF-2 with different lag-time films coating. The effect of coating times on the release of salmon sperm DNA in pH transition release experiments is summarized in Figure 7. With the increase of

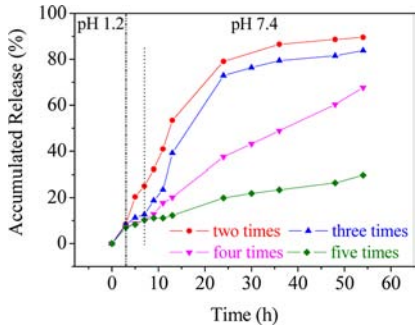

Figure 7. Salmon sperm DNA release profiles for pH transition from 1.2 to 7.4 (salmon sperm DNA-loaded ZrBF-2 with different lag-time films coating (two times, three times, four times, and five times)).

coating times, release of salmon sperm DNA in the simulated intestinal fluid (pH 7.4) could be obviously restrained and the release rate also gradually slows down. For two times coating, the initial release rate is higher than those of more times coating and 16.5% of salmon sperm DNA is released within 4 h, indicating that the loss of salmon sperm DNA in the small intestine cannot be ignored. With the coating times increasing from three to four, the release amount of salmon sperm DNA within 4 h decrease from 4.5% to 2.9%, respectively. Further increasing coating times to five, the release amount of salmon sperm DNA does not decrease within the equal time interval and the released salmon sperm DNA amount just reaches as low as 29.7% even though the release time prolongs to 54 h, showing release of salmon sperm DNA in the colon is extremely incomplete. From the above discussion, salmon sperm DNA-loaded ZrBF-2 with two times coating and five times coating cannot efficiently deliver salmon sperm DNA to the colon due to unignorable loss in the small intestine and extremely incomplete release in the colon, respectively. Hence, the release profiles of salmon sperm DNA-loaded ZrBF-2 with three times coating and four times coating are compared as follows. The significant difference of release behaviors between three times coating and four times coating appears after 4 h in the simulated intestinal fluid (pH 7.4). The salmon sperm DNA-loaded ZrBF-2 with three times coating exhibits a high release rate within 24 h (60.2% of the loaded amounts, from 7 to 24 h) followed by a slower liberation (10.9% of the loaded amounts, from 24 to 54 h), while salmon sperm DNA-loaded ZrBF-2 with four times coating almost displays a linear relationship between the release amount of salmon sperm DNA and the release time. Essentially, salmon sperm DNA-loaded ZrBF-2 with three times coating liberates salmon sperm DNA at a nonuniform release rate in the colon; however, salmon sperm DNA-loaded ZrBF-2 with four times coating always releases salmon sperm DNA at a uniform release rate. When the release time is up to 54 h, the release amount of salmon sperm DNA for salmon sperm DNA-loaded ZrBF-2 with three times coating and four times coating can reach 83.8% and 67.7%, respectively. The salmon sperm DNA-loaded ZrBF-2 with three times coating and four times coating can carry a large proportion of the loaded salmon sperm DNA to the colon with a minimum release of salmon sperm DNA when passing through the stomach and small intestine under dual control, time control, and pH value control. Thus, the time- and pH-controlled colon-targeted nucleic acid delivery systems have been developed by dip-coating lag-time films on pH-sensitive ZrBF-2 loading salmon sperm DNA.

Agarose gel electrophoresis tests were conducted to investigate the structural integrity of salmon sperm DNA in the delivery. As shown in Figure 8, the agarose gel electrophoresis image of salmon sperm DNA released from salmon sperm DNA-loaded ZrBF-2 with three times coating (lane 2) was compared with that of salmon sperm DNA before

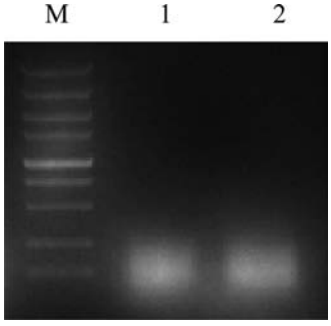

Figure 8. Agarose gel electrophoresis images of salmon sperm DNA before adsorption and after release from salmon sperm DNA-loaded ZrBF-2 with three times coating in the pH transition experiment (lane M, DL5000 DNA marker; lane 1, native salmon sperm DNA; lane 2: released salmon sperm DNA).

dx.doi.org/10.1021/ic3020942 | Inorg. Chem. 2013, 52, 1388−1397

adsorption (lane 1). The band of salmon sperm DNA after release is identical to that of salmon sperm DNA before adsorption even though salmon sperm DNA-loaded ZrBF-2 with three times coating has been immersed in acidic environment of pH 1.2 for 3 h, suggesting that salmon sperm DNA adsorbed into ZrBF-2 can be effectively protected against hydrolysis and preserve its integrated structure under acidic condition of the stomach.

The conformation of salmon sperm DNA after release was also studied through CD spectroscopy because the conformation of nucleic acid is inherently correlated to its biological activity. CD spectra of salmon sperm DNA which were released from salmon sperm DNA-loaded ZrBF-2 with three times coating in pH transition release experiment, and native salmon sperm DNA are displayed in Figure 9. Either the released

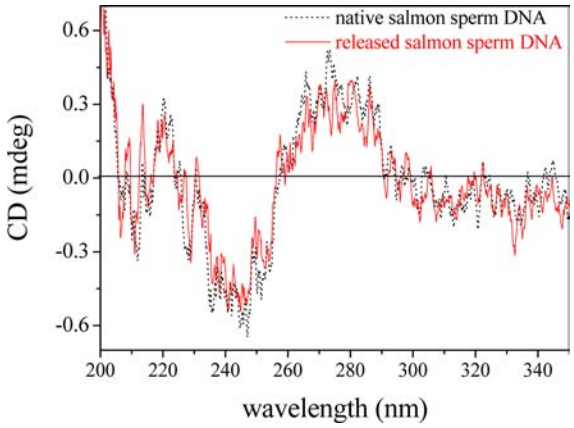

Figure 9. CD spectra of salmon sperm DNA released from salmon sperm DNA-loaded ZrBF-2 with three times coating and native salmon sperm DNA.

salmon sperm DNA or native salmon sperm DNA exhibits a positive Cotton effect at 280 nm and a negative Cotton effect at 240 nm, which is the same as those reported for B-form conformation of natural DNA.[42] In addition, the CD spectrum of the released salmon sperm DNA is almost similar to that of native salmon sperm DNA, showing that salmon sperm DNA can retain the B-form conformation during adsorption, coating of lag-time films, and pH transition release. The salmon sperm DNA adsorbed into ZrBF-2 may be mounted as an unraveled thread for mesopore confinement, which makes it so salmon sperm DNA cannot ravel in the mesopore void of ZrBF-2 and retain its native conformation without denaturation. The CD results suggest that salmon sperm DNA mounted into the mesopore of ZrBF-2 can be efficiently protected against denaturation even under the environment of gastric acid. Hence, salmon sperm DNA can remain intact without hydrolysis and denaturation during delivery, indicating that the time- and pH-controlled colon-targeted nucleic acid delivery system based on ZrBFs provides enough protection for nucleic acid.

3.4. Functionalization of ZrBFs. R8, a cell-penetrating peptide, was proved to have enhanced penetration capability through biomembranes[43] and to be used in functionalization of ZrBF-2. Scheme 2 illustrates that ZrBFs can be further functionalized with R8 using the coupling agent EDC/NHS through the carboxyls in L-proline groups of H_3PMP on the outer surface of samples. The functionalized sample, designated as salmon sperm DNA-loaded ZrBF-2-R8, was characterized by the fluorescence spectrum because guanidino of arginine in R8 can react with 9,10-phenanthraquinone in an alkaline medium, producing an intermediate compound which can easily be hydrolyzed in an acidic medium forming a fluorescent derivative and aldehyde.[44,45] The fluorescence (emission) spectra of the 9,10-phenanthraquinone derivative of free R8 and R8 from salmon sperm DNA-loaded ZrBF-2-R8 are shown in Figure 10 in comparison with that of salmon sperm DNA-

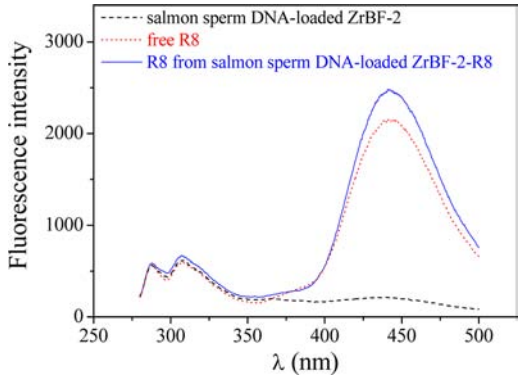

Figure 10. Fluorescence spectra of the 9,10-phenanthraquinone derivative of free R8 and R8 from salmon sperm DNA-loaded ZrBF-2-R8 in comparison with that of salmon sperm DNA-loaded ZrBF-2.

loaded ZrBF-2. Fluorescence emission at 442 nm can be observed for either free R8 or R8 from salmon sperm DNA-loaded ZrBF-2-R8, whereas no fluorescence emission appears for salmon sperm DNA-loaded ZrBF-2. The results of fluorescence spectra demonstrate that R8 has been coupled on the outer surface of salmon sperm DNA-loaded ZrBF-2 through amido bonds. Moreover, the amount of R8 linked with salmon sperm DNA-loaded ZrBF-2 can be determined according to the calibration graph (fluorescence intensity vs concentration of R8), 15.8 μg R8/1 mg salmon sperm DNA-loaded ZrBF-2.[34] The cell-penetrating peptide of R8 functionalized on the outer surface of the samples will enhance the penetration capability of ZrBFs through the biomembrane, which may help to improve the bioavailability of nucleic acids.

4. CONCLUSIONS

The bifunctional mesoporous zirconium phosphonates have been designed for oral colon-targeted delivery of nucleic acids through simultaneously incorporating two different phosphonic acids into the frameworks wherein the reversible protonation−deprotonation of L-proline groups of H_3PMP and piperazine groups of BPMP on the mesoporous walls under different pH values (pH sensitivity) as well as the further functionalization with cell-penetrating peptides via the carboxyl in L-proline group of H_3PMP on outer surface (functionalizability) endows the materials with pH-controllable release function and high cell penetration capability, respectively. ZrBFs also exhibit high surface area and large pore volume as well as tunable mesopore (2.4−14.0 nm), which favors high payload for nucleic acids. ZrBFs, possessing cationic frameworks once formed, adsorb and entrap negatively charged salmon sperm DNA in the mesopore through electrostatic attraction under acidic or neutral condition, whereas ZrBFs displaying anionic surface properties under weakly basic pH release negatively charged salmon sperm DNA for the appearance of electrostatic repulsion between them. The time- and pH-controlled colon-

dx.doi.org/10.1021/ic3020942 | Inorg. Chem. 2013, 52, 1388−1397

targeted nucleic acid delivery systems have been developed by dip-coating lag-time films on pH-sensitive ZrBFs loading salmon sperm DNA, which can effectively protect salmon sperm DNA intact in acidic medium of the stomach and efficiently deliver salmon sperm DNA to the colon. Furthermore, ZrBFs can be further functionalized with a cell-penetrating peptide of octaarginine (R8), which will enhance thr penetration capability of ZrBFs through biomembranes. Delivery of nucleic acids in such a way could improve delivery efficiency, bioactivity conservation, and bioavailability through dual control (time control and pH value control), lag-time films coating, and further functionalization with cell-penetrating peptides, respectively. ZrBFs as a new kind of carrier may have a promising application in oral delivery of nucleic acids targeting the colon for gene therapy of colon-related diseases.

■ ASSOCIATED CONTENT

Ⓢ Supporting Information

SEM and TEM images and ^{13}C CP/MAS NMR spectrum of BPMP. This material is available free of charge via the Internet at http://pubs.acs.org.

■ AUTHOR INFORMATION

Corresponding Author

*E-mail: xinshi@lnnu.edu.cn.

Author Contributions

†These authors contributed equally to this work.

Notes

The authors declare no competing financial interest.

■ ACKNOWLEDGMENTS

Financial support of this work was provided by the National Natural Science Foundation of China (21173108) and the National Basic Research Program of China (2009CB220010).

■ REFERENCES

(1) (a) Kraeling, M. E. K.; Ritschel, W. A. *Methods Find. Exp. Clin. Pharmacol.* **1992**, *14*, 199. (b) Sayani, A. P.; Chein, Y. W. *Crit. Rev. Ther. Drug Carrier Syst.* **1996**, *13*, 85. (c) Yamabe, K.; Kato, Y.; Onishi, H.; Machida, Y. *J. Controlled Release* **2003**, *89*, 429.

(2) (a) Gwinup, G.; Elias, A. N.; Domurat, E. S. *Gen. Pharmacol.* **1991**, *22*, 243. (b) Sah, H. K.; Toddywala, R.; Chien, Y. W. *J. Controlled Release* **1994**, *30*, 201. (c) Cleland, J. L.; Johnson, O. L.; Putney, S.; Jones, A. J. S. *Adv. Drug Delivery Rev.* **1997**, *28*, 71.

(3) (a) Bernkop-Schnurch, A. *J. Controlled Release* **1998**, *52*, 1. (b) Jung, T.; Kamm, W.; Breitenbach, A.; Kaiserling, E.; Xiao, J. X.; Kissel, T. *Eur. J. Pharm. Biopharm.* **2000**, *50*, 147. (c) Carino, G. P.; Mathiowitz, E. *Adv. Drug Delivery Rev.* **1999**, *35*, 249.

(4) (a) Cleland, J. L.; Daugherty, A.; Mrsny, R. *Curr. Opin. Biotechnol.* **2001**, *12*, 212. (b) van Dijkhuizen-Radersma, R.; Nicolas, H. M.; van de Weert, M.; Blom, M.; deGroot, K.; Bezemer, J. M. *Int. J. Pharm.* **2002**, *248*, 229. (c) Pan, Y.; Li, Y. J.; Zhao, H. Y.; Zheng, J. M.; Xu, H.; Wei, G.; Hao, J. S.; Cui, F. D. *Int. J. Pharm.* **2002**, *249*, 139. (d) Li, H.; Song, J. H.; Park, J. S.; Han, K. *Int. J. Pharm.* **2003**, *258*, 11.

(5) Hata, H.; Saeki, S.; Kimura, T.; Sugahara, Y.; Kuroda, K. *Chem. Mater.* **1999**, *11*, 1110.

(6) Vallet-Regí, M.; Rámila, A.; del Real, R. P.; Pérez-Pariente, J. *Chem. Mater.* **2001**, *13*, 308.

(7) Fisher, K. A.; Huddersman, K. D.; Taylor, M. J. *Chem.—Eur. J.* **2003**, *9*, 5873.

(8) Doadrio, A. L.; Sousa, E. M. B.; Doadrio, J. C.; Pérez-Pariente, J.; Izquierdo-Barba, I.; Vallet-Regí, M. *J. Controlled Release* **2004**, *97*, 125.

(9) Manzano, M.; Vallet-Regí, M. *J. Mater. Chem.* **2010**, *20*, 5593.

(10) Mellaerts, R.; Aerts, C. A.; Hummbeeck, J. V.; Augustijins, P.; Mooter, G. V.; Martens, J. A. *Chem. Commun.* **2007**, *13*, 1375.

(11) Doadrio, J. C.; Sousa, E. M. B.; Izquierdo-Barba, I.; Doadrio, A. L.; Pérez-Pariente, J.; Vallet-Regí, M. *J. Mater. Chem.* **2006**, *16*, 462.

(12) Andersson, J.; Rosenholm, J.; Areva, S.; Linden, M. *Chem. Mater.* **2004**, *16*, 4160.

(13) Yang, P. P.; Gai, S. L.; Lin, J. *Chem. Soc. Rev.* **2012**, *41*, 3679.

(14) Carino, I. S.; Pasqua, L.; Testa, F.; Aiello, R.; Puoci, F.; Iemma, F.; Picci, N. *Drug Delivery* **2007**, *14*, 491.

(15) Tang, Q. L.; Xu, Y.; Wu, D.; Sun, Y. H.; Wang, J.; Xu, J.; Deng, F. *J. Controlled Release* **2006**, *114*, 41.

(16) Song, S. W.; Hidajat, K.; Kawi, S. *Langmuir* **2005**, *21*, 9568.

(17) Lee, C. H.; Lo, L. W.; Mou, C. Y.; Yang, C. S. *Adv. Funct. Mater.* **2008**, *18*, 3283.

(18) Cheng, S. H.; Liao, W. N.; Chen, L. M.; Lee, C. H. *J. Mater. Chem.* **2011**, *21*, 7130.

(19) Gao, Q.; Xu, Y.; Wu, D.; Sun, Y. H.; Li, X. A. *J. Phys. Chem. C* **2009**, *113*, 12753.

(20) Hong, C. Y.; Li, X.; Pan, C. Y. *J. Mater. Chem.* **2009**, *19*, 5155.

(21) Xu, W. J.; Gao, Q.; Xu, Y.; Wu, D.; Sun, Y. H. *Mater. Res. Bull.* **2009**, *44*, 606.

(22) Xu, Y. P.; Qu, F. Y.; Wang, Y.; Lin, H. M.; Wu, X.; Jin, Y. X. *Solid State Sci.* **2011**, *13*, 641.

(23) Chen, F.; Zhu, Y. C. *Microporous Mesoporous Mater.* **2012**, *150*, 83.

(24) Song, S. W.; Hidajat, K.; Kawi, S. *Chem. Commun.* **2007**, *42*, 4396.

(25) Bhaumik, A.; Iangaki, S. *J. Am. Chem. Soc.* **2001**, *123*, 691.

(26) Ren, N.; Tang, Y.; Wang, Y. J.; Hu, S. H.; Dong, A. G.; Hua, W. M.; Yue, Y. H.; Shen, J. Y. *Chem. Lett.* **2002**, 1036.

(27) (a) Kimura, T. *Chem. Mater.* **2003**, *15*, 3742. (b) Kimura, T. *Chem. Mater.* **2005**, *17*, 337. (c) Kimura, T. *Chem. Mater.* **2005**, *17*, 5521. (d) Kimura, T.; Kato, K. *J. Mater. Chem.* **2007**, *17*, 559. (e) Kimura, T.; Kato, K. *Microporous Mesoporous Mater.* **2007**, *101*, 207.

(28) (a) El Haskouri, J.; Guillem, C.; Latoree, J.; Beltrán, A.; Beltrán, D.; Amorós, P. *Chem. Mater.* **2004**, *16*, 4359. (b) El Haskouri, J.; Guillem, C.; Latorre, J.; Beltrán, A.; Beltrán, D.; Amorós, P. *Eur. J. Inorg. Chem.* **2004**, 1804.

(29) (a) Ma, T. Y.; Yuan, Z. Y. *Chem. Commun.* **2010**, *46*, 2325. (b) Ma, T. Y.; Lin, X. Z.; Yuan, Z. Y. *J. Mater. Chem.* **2010**, *20*, 7406.

(30) Turner, A.; Jaffrès, P. A.; MacLean, E. J.; Villemin, D.; Mckee, B.; Hix, G. B. *Dalton Trans.* **2003**, 1314.

(31) Moedritzer, K.; Irani, R. R. *J. Org. Chem.* **1966**, *31*, 1603.

(32) Langmuir, I. *J. Am. Chem. Soc.* **1918**, *40*, 1362.

(33) Freundilich, H. M. F. *Z. Phys. Chem.* **1906**, *57*, 385.

(34) Abdel-Hay, M. H.; Galal, S. M.; Bedair, M. M.; Gazy, A. A.; Wahbi, A. A. M. *Talanta* **1992**, *39*, 1369.

(35) (a) Jaroniec, M.; Kruk, M.; Ryoo, R.; Joo, S. H. *Chem. Mater.* **2000**, *12*, 1414. (b) Jaroniec, M.; Kruk, M. *Chem. Mater.* **2001**, *13*, 3169.

(36) Shi, X.; Liu, J.; Li, C. M.; Yang, Q. H. *Inorg. Chem.* **2007**, *46*, 7944.

(37) Shi, X.; Li, J. P.; Tang, Y.; Yang, Q. H. *J. Mater. Chem.* **2010**, *20*, 6495.

(38) Shi, X.; Yang, J.; Yang, Q. H. *Eur. J. Inorg. Chem.* **2006**, 1936.

(39) Kaus, L. C.; Fell, J. T.; Sharma, H.; Taylor, D. C. *Int. J. Pharm.* **1984**, *14*, 143.

(40) Davis, S. S.; Hardy, J. G.; Fara, J. W. *Gut* **1986**, *27*, 886.

(41) Hinton, J. M.; Lennard-Jonnes, J. E.; Young, A. C. *Gut* **1969**, *10*, 842.

(42) Fiel, R. J.; Howard, J. C.; Mark, E. H.; Gupta, N. D. *Nucleic Acids Res.* **1979**, *6*, 3093.

(43) Rothbard, J. B.; Garlington, S.; Lin, Q.; Kirschberg, T.; Kreider, E.; McGrance, P. L.; Wender, P. A.; Khavari, P. A. *Nat. Med.* **2000**, *6*, 1253.

(44) Itano, H. A.; Yamada, S. *Anal. Biochem.* **1972**, *48*, 483.

(45) Tanabe, S.; Sakaguchi, T. *Chem. Pharm. Bull.* **1978**, *26*, 337.